Journal of Organometallic Chemistry 693 (2008) 2856–2862

Contents lists available at ScienceDirect

Journal of Organometallic Chemistry

journal homepage: www.elsevier.com/locate/jorganchem

Rearrangement and decomposition of $(CH_3)_3M^+$ (M = Si, Ge, Sn) ions: A DFT study

Igor S. Ignatyev [a], Tom Sundius [b,*]

[a] Department of Chemistry, Radiochemistry Laboratory, St. Petersburg State University, St. Petersburg 199034, Russia
[b] Department of Physics, University of Helsinki, P.O. Box 64, FIN-00014 Helsinki, Finland

ARTICLE INFO

Article history:
Received 3 March 2008
Received in revised form 27 May 2008
Accepted 2 June 2008
Available online 7 June 2008

Keywords:
Silylium
Germylium
Stannylium
Decomposition
DFT

ABSTRACT

Pathways for the rearrangement and decomposition of the $(CH_3)_3M^+$ (M = Si, Ge, Sn) ions are traced by the detection of stationary points on the potential energy surfaces of these ions by the B3LYP/aug-cc-pVDZ method. All three systems have stationary points similar in geometry, but very different in energy, especially on going from M = Si, Ge on the one hand to M = Sn on the other. In addition to previously found isomers of $(CH_3)_3Si^+$ which have their analogs in the two other systems, "side-on" complexes with ethane and propane were revealed for all cations studied. Predicted changes in transition state and dissociation energies on going from M = Si to M = Sn allowed us to rationalize the trends for the relative decomposition product yields observed in mass-spectrometry studies of these cations.

1. Introduction

Considerable difference is observed between chemical and physical properties of silicon and its heavier congeners, i.e. germanium and tin [1]. Particularly, for trivalent R_3M^+ cations this difference manifests itself in the growth of the relative stability of "side-on" structures, as shown by quantum chemical methods for the MH_3^+ cations (M = Si, Ge, Sn, and Pb) [2]. The other trend observed in the series of R_3M^+ cations on going from Si to Pb is the drastic change in the relative abundance of decomposition products. Mass analyzed ion kinetic studies of the fragmentation products of the $(CH_3)_3M^+$ ions by Groenewold et al. [3] revealed a small decrease of ethylene loss (accompanied by an increase of ethane and methyl radical elimination) on going from M = Si to M = Ge but complete absence of ethylene dissociation and a huge growth of the CH_3 elimination for M = Sn.

To the best of our knowledge there were no attempts to analyze the mechanisms of rearrangements and fragmentation for germylium or stannylium cations, although there exists numerous experimental [3–9,13] and theoretical [4,10–14] studies of similar processes for silylium ions. However in these studies no attention was paid to the possibility of formation of the "side-on" structures, which in the case of cations containing methyl groups manifest themselves as complexes with alkanes. In our previous communication [15] we considered these complexes for $(CH_3)_nH_{(3-n)}M^+$ ions with $n = 1,2$ and M = Si, Ge. It was shown that complexes with methane and ethane for M = Si lie substantially higher than those with ethylene, although they are lowering on going to germylium ions. Furthermore, on going from Si to Ge a considerable decrease of the barrier heights for their transformation from the most stable isomer was observed. Thus one may expect that in keeping with results of Kapp et al. [2] the "side-on" complexes with ethane as well as the barriers to their rearrangement will become even lower for stannyl ions. Hence the aim of the present work is to find similarities and differences in the profiles of isomerization and decomposition reactions of $(CH_3)_3M^+$ ions for M = Si, Ge, Sn in order to rationalize the trends in the decomposition product yields observed in mass-spectrometry studies.

2. Computational methods

The geometries of all of the stationary points have been fully optimized and characterized by harmonic vibrational frequency calculations using the B3LYP [16–17] hybrid density functional method as implemented in the GAUSSIAN03 program [18]. Since the parameters of the B3 exchange functional [16] have been fit only to first- and second-row compounds and may be less accurate for tin compounds, we assessed the accuracy of different basis sets in reproduction of a few existing experimental parameters of potential energy surfaces of methyl-containing tin compounds, i.e. the bond length and vibrational spectrum of $Sn(CH_3)_4$ [19,20].

For the most important stationary points which determine the output of decomposition products, i.e. transition states TS1 and

* Corresponding author. Tel.: +358 9 191 50672; fax: +358 9 191 50610.
E-mail address: Tom.Sundius@helsinki.fi (T. Sundius).

0022-328X/$ - see front matter © 2008 Elsevier B.V. All rights reserved.
doi:10.1016/j.jorganchem.2008.06.006

TS2, as well as the homolytic dissociation level, optimization at the MP2 (frozen core) [21] and density functional BMK [22] methods was carried out.

Results of the comparison of these experimental parameters with those obtained by the B3LYP method with different basis sets are shown in Table 1. First three basis sets include a valence double-ζ set with an ECP and relativistic corrections denominated as LANL2DZ [23–25] for tin and D95V [26] for first row atoms as well as the same set for Sn, but with cc-pVDZ and aug-cc-pVDZ [27,28] sets for H and C. The other two are the Peterson's sets with small-core relativistic pseudopotentials [29] for Sn (cc-pVDZ-PP and aug-cc-pVDZ-PP) and corresponding Dunning correlation-consistent sets for C and H. The results obtained with MP2 and BMK methods employing LANL2DZ- aug-cc-pVDZ basis set were also included in Table 1. The comparison of the performance of these basis sets and methods in the reproduction of vibrational frequencies (CH stretching frequencies are not included due to their large anharmonicity) and the SnC bond length (Table 1) demonstrates that sets with LANL2DZ for Sn and D95V for other elements as well as cc-pVDZ-PP of Peterson give the largest discrepancies between the calculated and experimental vibrational frequencies. Other methods give much better and almost similar results in the description of vibrational frequencies. However, among them the basis set denominated as LANL2DZ-aug-cc-pVDZ gives the best results in the description of experimental SnC bond length and it is used for the location of stationary points at the potential energy surface of trimethylstannylium cation. For silylium and germylium ions the aug-cc-pVDZ basis set is used for all atoms.

The IRC path following for the descent from the barrier top was employed to determine energy minima, which are connected by a particular transition state. Zero-point vibrational energy corrections (ZPVE) were estimated at the same theory level at which optimization was carried out and E_0 was calculated as E_e (total energy at equilibrium geometry) + ZPVE.

3. Results and discussion

3.1. Trimethylsilylium ion

The existence of side-on complexes, which was demonstrated for the SiH_3^+ cation [2], was not taken into account in the analysis of the potential energy surfaces of silylium ions containing alkyl groups [10–14] before our previous communication [15] in which we found energy minima corresponding to methane and ethane complexes at the potential energy surface of H_5CSi^+ and $H_7C_2Si^+$ systems. These complexes may be derived from the side-on complexes found by Kapp et al. [2] in H_3Si^+ and H_3Ge^+ cations by the methyl substitution of the dihydrogen moiety atoms. In the $H_7C_2Si^+$ system the methane complex lies 28.5 kcal/mol higher in energy than the most stable isomer and the complex with ethane lies 45.4 kcal/mol higher. However, they are separated from the main isomer by substantially high barriers, namely 71.1 and 88.8 kcal/mol, respectively (B3LYP/aug-cc-pVDZ).

For the $H_9C_3Si^+$ system the ethane complex (**3**, Fig. 1) was found lying 45.0 kcal/mol (hereafter B3LYP E_0 values will be used as energy characteristics of the stationary points) higher than the most stable form $(CH_3)_3Si^+$ (Table 2). Earlier characterized isomers **2** and **4** are substantially more stable than **3**. Moreover, the transformation from **1** to **3** requires overcoming the barrier **TS2**, which is 95.3 kcal/mol high (Fig. 1, Table 2). This explains the very low yield of ethane among the products of the $(CH_3)_3Si^+$ cation decomposition [3] despite the fact that the ethane elimination energy level lies slightly lower than that for the loss of ethylene (Table 2, Scheme 1).

Earlier, in the studies in which the ethane complex was not located [11–13] it was proposed that the transition state with symmetric displacement of two hydrogens from silicon to the ethylene moiety (**TS4** in Fig. 1) connects directly the ethylene complex **4** with the most stable tertiary isomer **1**. However, in this study we found that this transition state connects these structures with the intermediacy of the ethane complex (**1** ↔ **TS2** ↔ **3** ↔ **TS4** ↔ **4**, Fig. 1, Scheme 1). To follow this path the system needs to overcome a high barrier **TS2**, although another transition state (earlier described by Ketvirtis et al. [10]) was found which connects **1** and **4** through the second most stable isomer **2** (**1** ↔ **TS1** ↔ **2** ↔ **TS3** ↔ **4**, Fig. 1, Scheme 1). The highest barrier on this path (**TS1**), is substantially lower than **TS2** (Table 2).

The ethane complex **3** may transform also through the barrier **TS5** into the propane complex **5**. However, this path requires large energy: the C_3H_8 dissociation energy level lies substantially higher than the levels for the ethane and ethylene elimination (Table 2, Scheme 1).

Table 1
Experimental vibrational frequencies[a] (cm^{-1}) and the bond length[b] (Å) of $SnMe_4$ compared to theoretical values obtained with B3LYP method with LANL2DZ basis set for Sn and different basis sets

Exp.[a,b]	[c]	[d]	[e]	[f]	[g]	MP2	BMK	Description
1442	1505	1450	1437	1494	1442	1449	1444	F_2 δ_{as} CH_3
1442	1496	1440	1427	1484	1434	1438	1433	E δ_{as} CH_3
	1494	1438	1425	1482	1431	1436	1430	F_1 δ_{as} CH_3
1204	1311	1239	1240	1268	1224	1245	1243	A_1 δ_s CH_3
1203	1301	1225	1231	1257	1212	1231	1230	F_2 δ_s CH_3
777	838	781	777	796	781	773	774	F_2 ρ CH_3
771	824	776	774	794	779	772	768	E ρ CH_3
	709	666	664	689	678	647	645	F_1 ρ CH_3
530	530	511	514	513	511	526	522	F_2 ν SnC
508	502	485	488	483	480	505	505	A_1 ν SnC
146	156	153	149	144	143	139	140	F_2 δ CSnC
147	144	141	135	135	134	124	124	E δ CSnC
102	107	121	113	108	121	113	89	F_1 τ CH_3
102	104	121	105	106	130	89	63	A_2 τ CH_3
	54	17	17	34	16	17	20	RMS error
2.144	2.148	2.149	2.148	2.182	2.178	2.144	2.139	SnC bond

[a] Vibrational frequencies are from Ref. [20].
[b] The SnC bond length is from Ref. [19].
[c] LANL2DZ for Sn, D95V for H,C.
[d] LANL2DZ for Sn, cc-pVDZ for H,C.
[e] LANL2DZ for Sn, aug-cc-pVDZ for H,C.
[f] cc-pVDZ-PP for Sn, cc-pVDZ for H,C.
[g] aug-cc-pVDZ-PP for Sn, aug-cc-pVDZ for H,C.

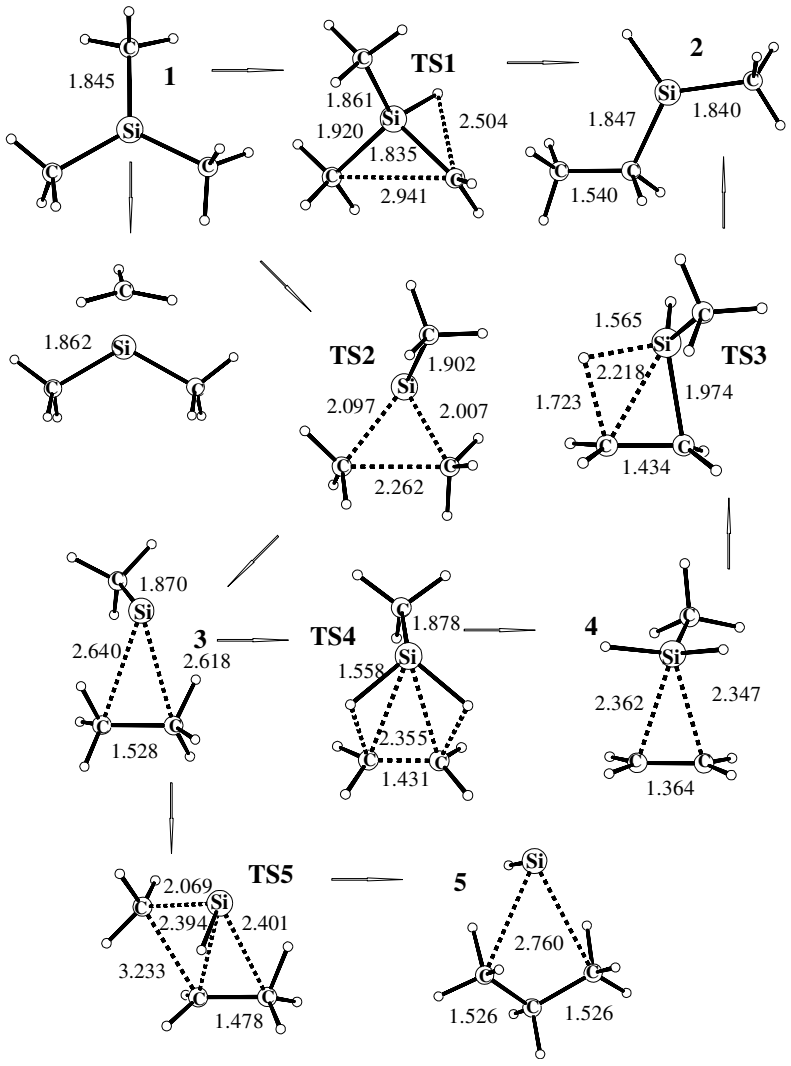

Fig. 1. Equilibrium structures (bond lengths in Å) of stationary points found at the $H_9C_3Si^+$ potential energy surface.

The other decomposition channel, which was not regarded before, is the homolytic cleavage of the SiC bond producing methyl radical and dimethylsilylene radical cation. This is a high-energy process (89.4 kcal/mol), however this dissociation level lies slightly lower than the barrier **TS2** for the transformation into the ethane complex **3** (Table 2, Scheme 1).

3.2. Trimethylgermylium ion

Structure of stationary points at the potential energy surface of this system is similar to that of the corresponding states for the $H_9C_3Si^+$ ion (Figs. 1 and 2). The $H_9C_3Ge^+$ system is characterized by longer M–C bonds and the asymmetry of the **TS4** structure.

Larger changes on going from Si to Ge may be observed in the relative energies of these states (Table 2). For instance, both the energy level for the homolytic SiC scission and the **TS2** barrier height substantially decrease, while the barrier **TS1** on the path leading to ethylene elimination increases. This tendency is in keeping with the observed small decrease (from 75.0% to 73.8%) of the relative abundance of ethylene loss (**TS1** is still the lowest barrier) and an increase of that of CH_3 (from 2.6% to 11.9%) as well as C_2H_6 (from 1.9% to 9.5%).

3.3. Trimethylstannylium ion

All stationary points, which were found for $H_9C_3Si^+$ and $H_9C_3Ge^+$, were also located at the $H_9C_3Sn^+$ potential energy surface. However, the geometry and energy parameters of these points differ substantially from those of previous systems. First, the order of stability of isomers has changed: the second most stable isomer is no longer the secondary ion designated as **2**, but rather the ethane complex **3**. The energy of the propane complex **5** also drops drastically on going from M = Si to M = Sn and in the $H_9C_3Sn^+$ system it becomes the third most stable isomer, thus shifting the ethylene complex **4** to the fourth position. The reason of this large increase in the stability of the ethane and propane complexes as well as the lowering of corresponding dissociation levels is the significant increase of the stability of monovalent cations HM^+ and MeM^+ on going from M = Si to M = Sn. This effect is due to the increase of the energy difference between valence s and p electrons and the decrease of their hybridization on going down group 14. One of the consequences is the ease with which the heavier group 14 elements form low-valent species [31]. There are also significant changes in the energies of transition states, the most important of which is the substantial lowering of the **TS2** barrier height. As a result the **TS1** and **TS2** energy levels become nearly equal

Table 2
Relative energies (ΔE_e, $\Delta E_0 = \Delta E_e + \Delta ZPVE$, kcal/mol) of stationary points at the PES of $(CH_3)_3M^+$ (M = Si, Ge, Sn) cations

Structure[a]	Si		Ge		Sn	
	ΔE_e	ΔE_0	ΔE_e	ΔE_0	ΔE_e	ΔE_0
B3LYP/LANL2DZ-aug-cc-pVDZ						
1	0	0	0	0	0	0
$CH_3^{\cdot} + (CH_3)_2M^{+\cdot}$	94.6	89.4	82.7	77.7	70.0	65.4
TS1	61.4	59.1	65.6	62.9	72.6	68.8
2	19.7	19.7	15.9	15.6	13.3	13.1
TS2	95.9	95.3	81.9	81.0	71.2	71.0
3	44.5	45.0	21.8	22.4	3.9	5.3
$C_2H_6 + (CH_3)M^+$	57.8	57.2	34.1	33.9	13.0	13.8
TS3	38.1	37.1	39.1	37.6	42.0	39.8
TS4	68.5	66.2	59.3	56.4	58.0	54.8
4	28.7	27.9	25.1	23.9	23.1	21.0
$C_2H_4 + (CH_3)H_2M^+$	64.3	60.1	57.3	52.9	50.0	45.3
TS5	90.7	90.5	73.4	72.6	65.6	64.4
5	62.3	62.6	36.1	36.6	15.0	16.1
$C_3H_8 + HM^+$	87.9	87.4	58.7	58.4	32.0	32.3
MP2/LANL2DZ-aug-cc-pVDZ						
1	0	0	0	0	0	0
$CH_3^{\cdot} + (CH_3)_2M^{+\cdot}$	98.7	95.0	90.7	87.7	73.5	71.3
TS1	68.4	66.3	72.4	69.8	80.7	77.0
TS2	98.6	98.0	89.8	89.1	76.6	76.5
BMK/LANL2DZ-aug-cc-pVDZ						
1	0	0	0	0	0	0
$CH_3^{\cdot} + (CH_3)_2M^{+\cdot}$	103.6	98.3	92.3	86.8	77.6	72.8
TS1	64.9	62.8	71.4	68.6	78.2	74.4
TS2	101.2	101.1	90.8	90.0	80.6	80.7

[a] Structure numbering as in Figs. 1–3.

(Scheme 2). There are also significant decreases in the **TS4** and **TS5** barrier heights, especially for the latter. Note also the important decrease of the dissociation energy for the M–C bond homolytic cleavage on going from M = Si to M = Sn (Table 2).

3.4. Comparison of predicted decomposition mechanisms with experimental results

The obtained thermochemical characteristics of the $H_9C_3M^+$ (M = Si,Sn) allows us to rationalize the observed relative yields of decomposition products for these cations [3].

Among the mass analyzed ion kinetic energy (MIKE) unimolecular decomposition products of $(CH_3)_3Si^+$ the loss of C_2H_4 dominates. This fact allowed Groenewold et al. [3] to propose that this low-energy decomposition proceeds through a rearrangement. However, the increased loss of ethylene after collisional activation (CA) was ascribed by these authors to the fact that the other kind of rearrangement (with high-energy activation state) may be operative in the CA experiments. Note that the increased loss of C_2H_4 is accompanied by the more significant increase in the C_2H_6 elimination which was close to zero in the MIKE unimolecular decomposition experiment.

This feature may be well explained by the analysis of our results (Table 2, Scheme 1). For $(CH_3)_3Si^+$ the lowest barrier on the paths leading to decomposition products is **TS1** which through **2** ↔ **TS3** ↔ **4** (Fig. 1) leads to the dissociation with the loss of ethylene. The height of the **TS1** barrier (59.1 kcal/mol) is rate determining, since the other barrier on this path (**TS3**) has a substantially lower barrier (37.1 kcal/mol). The other path leading to the ethylene elimination is that going through the sequence **TS2** ↔ **3** ↔ **TS4** ↔ **4**. The first step on this path has a high-energy barrier (95.3 kcal/mol) which system may overcome only in the CA experiment. However this path leads firstly to the ethane complex, which may dissociate with the release of C_2H_6 since this dissociation energy is close to the barrier height (**TS4**) on the further path to the ethylene release.

There are small changes in low-energy MIKE decomposition product yields on going from M = Si to M = Ge: the relative abundance of the C_2H_4 loss diminishes from 75% to 74%, but this value for C_2H_6 grows up to 10%. The substantial increase is observed for the CH_3 loss (from 3% to 12%). These changes are more pronounced in the high-energy CA experiments, in which the relative abundances of CH_3 and C_2H_6 achieve 26% and 37%, respectively, while that of C_2H_4 drops to 8%.

These changes may be associated with the increase of the **TS1** energy and the lowering of the **TS2** barrier height. The increase of the methyl radical yield may be rationalized taking into account the decrease of the homolytic scission energy from 89.4 kcal/mol for M = Si to 77.7 kcal/mol for M = Ge (Table 2).

On going from M = Si, Ge to M = Sn the relative abundance of decomposition products changes radically. There is no more ethylene loss products among decomposition products, but in the MIKE unimolecular decomposition CH_3 (75%) dominates with a smaller yield of C_2H_6 (13%). In the high-energy CA experiment the output of these products becomes equal (39%) and noticeable yields of C_3H_8 (8%) and C_3H_9 (11%) are observed.

These drastic differences in the $(CH_3)_3Si^+$ and $(CH_3)_3Sn^+$ decomposition product yields may be rationalized by the analysis of the predicted energies presented in Schemes 1 and 2. First, from three channels of the decomposition of $(CH_3)_3Sn^+$ (Fig. 3) the homolytic cleavage of the SnC bond producing the methyl radical becomes the lowest one. Two other paths proceeding through barriers **TS1**

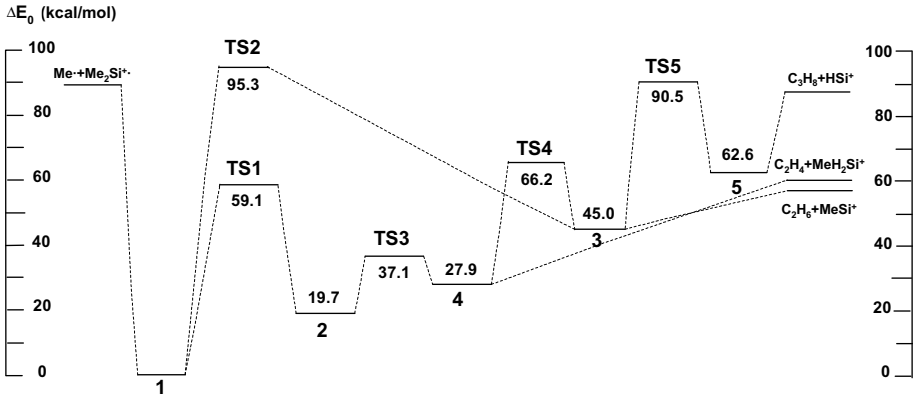

Scheme 1. Energy levels (kcal/mol) of stationary points at the $H_9C_3Si^+$ potential energy surface.

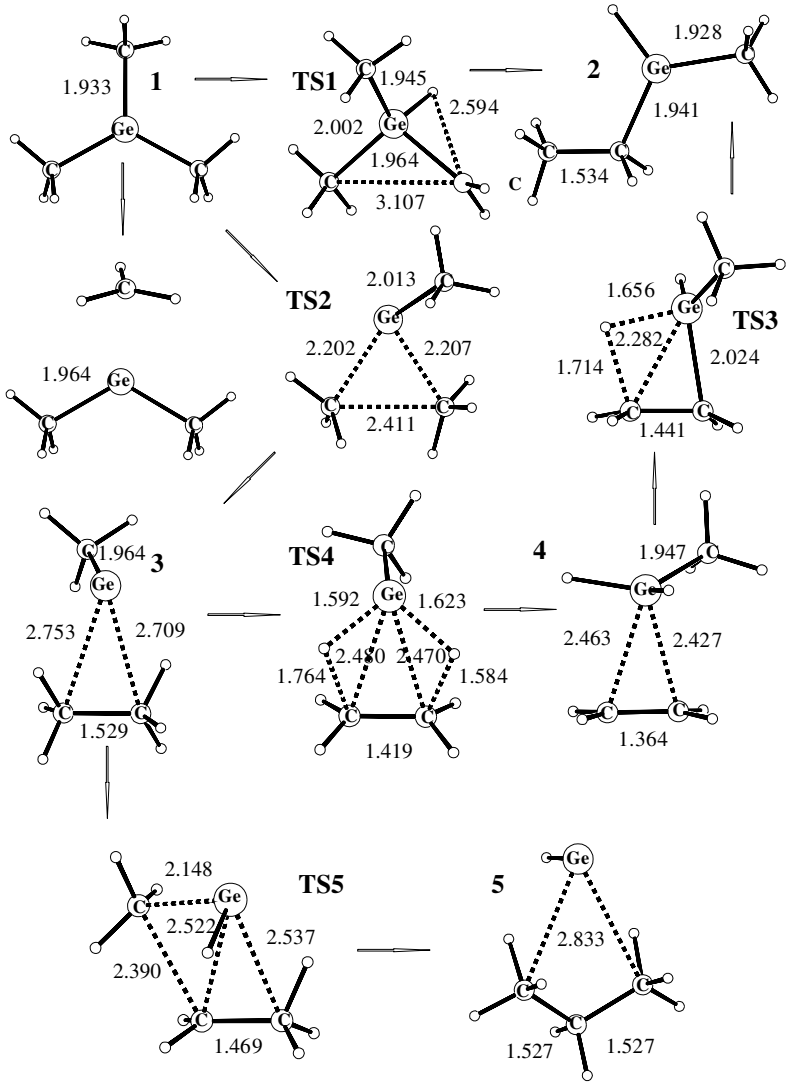

Fig. 2. Equilibrium structures (bond lengths in Å) of stationary points found at the $H_9C_3Ge^+$ potential energy surface.

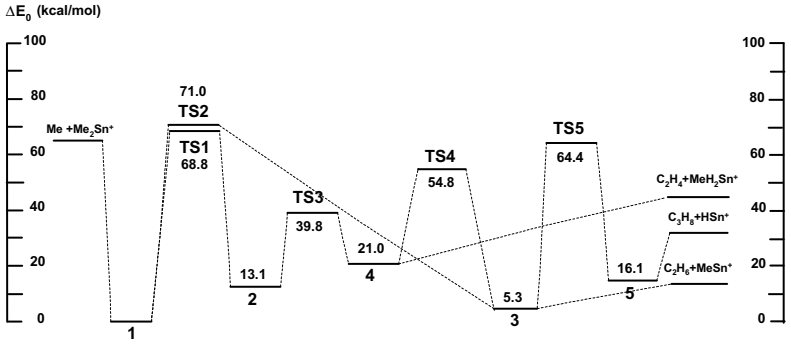

Scheme 2. Energy levels (kcal/mol) of stationary points at the $H_9C_3Sn^+$ potential energy surface.

and **TS2** have close values of their heights: in terms of E_e **TS2** is lower, but taking ZPVE into account reverses this relation. However, if we assume that the accuracy of the estimation of barrier heights in the B3LYP/aug-cc-pVDZ method may be no less than 5–7 kcal/mol [30], it is possible that **TS2** may be somewhat lower than **TS1**. The tendency to this display the MP2 results (Table 2). With this method the **TS2** barrier height is slightly lower than that of **TS1**, while another DFT method employed, i.e. BMK, gives their ratio similar to that of B3LYP (Table 2). This is the only difference between MP2 results and those of B3LYP. In general MP2 and BMK demonstrate slightly higher barrier heights and homolytic dissociation levels but their relative values remain similar to those obtained by B3LYP (with one exception discussed above). Note also the inversion of the dissociation energy levels depicted at the right

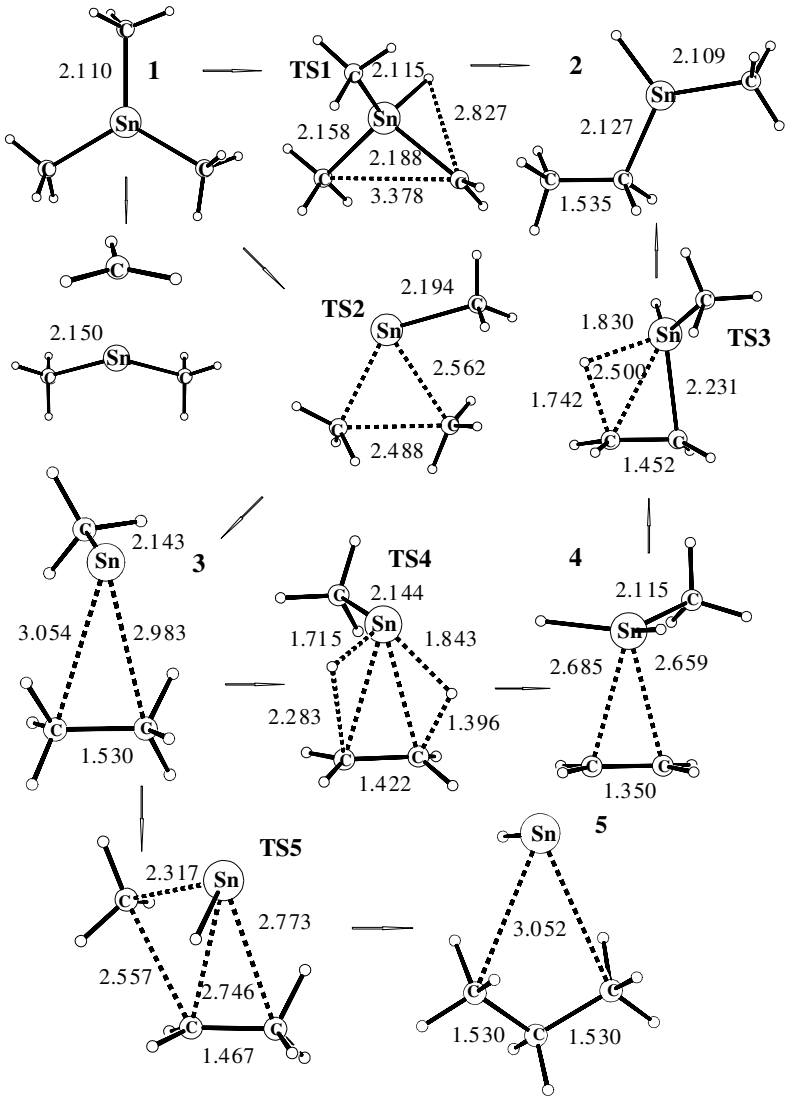

Fig. 3. Equilibrium structures (bond lengths in Å) of stationary points found at the $H_9C_3Sn^+$ potential energy surface.

side of Schemes 1 and 2: that of the ethylene elimination in M = Sn becomes the highest one and lies above the corresponding level for the propane elimination.

4. Conclusions

1. Similar mechanisms of the rearrangement and decomposition for all the $(CH_3)_3$ M^+ ions (M = Si, Ge, Sn) were found, however, the energy characteristics of the stationary points on their paths differ significantly for M = Si and Ge on the one hand and M = Sn on the other.
2. The channels for these rearrangements involve the intermediacy of "side-on" complexes: not only the previously described ethylene complex but also the ethane and propane complexes not reported before.
3. Rearrangements of the tertiary $(CH_3)_3M^+$ ions may proceed through three channels: (i) conversion to the secondary cation with a subsequent transformation of it to the ethylene complex, (ii) isomerization to the ethane complex, which may be followed by transformations into ethylene and propane complexes, (iii) the homolytic cleavage of the SiC bond producing methyl radical and dimethylsilylene radical cation.
4. The energy of the homolytic cleavage (channel III) being substantially higher than the barrier for channel I in the M = Si and Ge systems becomes lower than the barrier heights for both channels I and II in the case of M = Sn.
5. The barrier for process I being substantially lower than that of II for M = Si and Ge becomes of nearly the same energy for M = Sn.
6. The order of the energies of the heterolytic dissociation with the formation of ethylene and alkanes changes on going from Si ($C_3H_8 > C_2H_4 > C_2H_6$) to Sn ($C_2H_4 > C_3H_8 > C_2H_6$).

Acknowledgement

We thank the Center for Scientific Computing in Espoo, Finland for the allotment of computer time.

References

[1] M. Karni, Y. Apeloig, in: Z. Rappoport, Y. Apeloig (Eds.), The Chemistry of Organic Silicon Compounds, 3, Wiley, New York, 2001.
[2] J. Kapp, P.R. Schreiner, P.v.R. Schleyer, J. Am. Chem. Soc. 118 (1996) 12154.
[3] G.S. Groenewold, M.L. Gross, M.M. Bursey, P.R. Jones, J. Organomet. Chem. 235 (1982) 165.
[4] Y. Apeloig, M. Karni, A. Stanger, H. Schwarz, T. Drewello, G. Czekay, J. Chem. Soc., Chem. Commun. (1987) 989.

[5] K.A. Reuter, D.B. Jacobson, Organometallics 8 (1989) 1126.
[6] T. Drewello, P.C. Burgers, W. Zummaek, Y. Apeloig, H. Schwartz, Organometallics 9 (1990) 1161.
[7] C.M. Holznagel, R. Bakhtiar, D.B. Jacobson, J. Am. Soc. Mass Spectrom. 2 (1991) 278.
[8] R. Bakhtiar, C.M. Holznagel, D.B. Jacobson, Organometallics 12 (1993) 880.
[9] R. Bakhtiar, C.M. Holznagel, D.B. Jacobson, Organometallics 12 (1993) 621.
[10] A.E. Ketvirtis, D.K. Bohme, A.C. Hopkinson, Organometallics 14 (1995) 347.
[11] I.S. Ignatyev, T. Sundius, Organometallics 15 (1996) 5674.
[12] I.S. Ignatyev, T. Sundius, Organometallics 17 (1998) 2819.
[13] B.B. Willard, S. T Graul, J. Phys. Chem. A 102 (1998) 6942.
[14] T.A. Kochina, D.A. Vrazhnov, I.S. Ignatyev, J. Organomet. Chem. 586 (1999) 241.
[15] I.S. Ignatyev, T.A. Kochina, D.A. Vrazhnov, Russ. J. Gen. Chem. 77 (2007) 575.
[16] A.D. Becke, J. Chem. Phys. 98 (1993) 5648.
[17] C. Lee, W. Yang, R.G. Parr, Phys. Rev. B 37 (1988) 785.
[18] M.J. Frisch, G.W. Trucks, H.B. Schlegel, G.E. Scuseria, M.A. Robb, J.R. Cheeseman, J.A. Montgomery Jr., T. Vreven, K.N. Kudin, J.C. Burant, J.M. Millam, S.S. Iyengar, J. Tomasi, V. Barone, B. Mennucci, M. Cossi, G. Scalmani, N. Rega, G.A. Petersson, H. Nakatsuji, M. Hada, M. Ehara, K. Toyota, R. Fukuda, J. Hasegawa, M. Ishida, T. Nakajima, Y. Honda, O. Kitao, H. Nakai, M. Klene, X. Li, J.E. Knox, H.P. Hratchian, J.B. Cross, C. Adamo, J. Jaramillo, R. Gomperts, R.E. Stratmann, O. Yazyev, A.J. Austin, R. Cammi, C. Pomelli, J.W. Ochterski, P.Y. Ayala, K. Morokuma, G.A. Voth, P. Salvador, J.J. Dannenberg, V.G. Zakrzewski, S. Dapprich, A.D. Daniels, M.C. Strain, O. Farkas, D.K. Malick, A.D. Rabuck, K. Raghavachari, J.B. Foresman, J.V. Ortiz, Q. Cui, A.G. Baboul, S. Clifford, J. Cioslowski, B.B. Stefanov, G. Liu, A. Liashenko, P. Piskorz, I. Komaromi, R.L. Martin, D. J. Fox, T. Keith, M.A. Al-Laham, C.Y. Peng, A. Nanayakkara, M. Challacombe, P.M. Gill, B. Johnson, W. Chen, M.W. Wong, C. Gonzalez, J.A. Pople, GAUSSIAN 03, Gaussian, Inc., Wallingford, CT, 2004.
[19] M. Nagashima, H. Fujii, M. Kimura, Bull. Chem. Soc. Jpn. 46 (1973) 3708.
[20] C. Manzanares, J. Peng, V.M. Blunt, J. Phys. Chem. 96 (1992) 6212.
[21] J.S. Binkley, J.A. Pople, Int. J. Quantum Chem. 9 (1975) 229.
[22] A.D. Boese, J.M.L. Martin, J. Chem. Phys. 121 (2004) 3405.
[23] P.J. Hay, W.R. Wadt, J. Chem. Phys. 82 (1985) 270.
[24] P.J. Hay, W.R. Wadt, J. Chem. Phys. 82 (1985) 284.
[25] P.J. Hay, W.R. Wadt, J. Chem. Phys. 82 (1985) 299.
[26] T.H. Dunning, P.J. Hay, in: H.F. Schaefer (Ed.), Modern Theoretical Chemistry, 3, Plenum, New York, 1976.
[27] D.E. Woon, T.H. Dunning, J. Chem. Phys. 98 (1993) 1358.
[28] T.H. Dunning, J. Phys. Chem. A 104 (2000) 9062.
[29] K.A. Peterson, J. Chem. Phys. 119 (2003) 11099.
[30] I.S. Ignatyev, H.F. Schaefer, J. Am. Chem. Soc. 126 (2004) 14515.
[31] G. Bertrand, Science 305 (2004) 783.